ACS OMEGA

http://pubs.acs.org/journal/acsodf

Article

Toward a Realistic Model of Diffusion-Limited Aggregation: Rotation, Size-Dependent Diffusivities, and Settling

Matteo Polimeno, Changho Kim,* and François Blanchette*

Cite This: *ACS Omega* 2022, 7, 40826−40835

Read Online

ACCESS | Metrics & More | Article Recommendations | Supporting Information

ABSTRACT: In this Brownian dynamics simulation study on the formation of aggregates made of spherical particles, we build on the well-established diffusion-limited cluster aggregation (DLCA) model. We include rotational effects, allow diffusivities to be size-dependent as is physically relevant, and incorporate settling under gravity. We numerically characterize the growth dynamics of aggregates and find that their radius of gyration, R_g, grows approximately as $R_g \sim t^{1.02}$ for classical DLCA but slows to an approximate growth rate of $R_g \sim t^{0.71}$ when diffusivity is size-dependent. We also analyze the fractal structure of the resulting aggregates and find that their fractal dimension, d, decreases from $d \approx 1.8$ for classical DLCA to $d \approx 1.7$ when size-dependent rotational diffusion is included. The addition of settling effects further reduces the fractal dimension observed to $d \approx 1.6$ and appears to result in aggregates with a vertical extent marginally smaller than their horizontal extent.

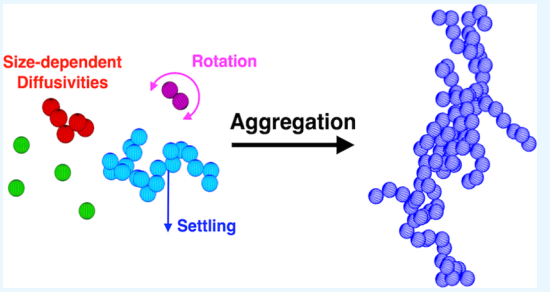

1. INTRODUCTION

The aggregation of small particles into larger clusters occurs in a great variety of contexts. It has been reported in metallic crystal[1,2] and aerogel formation,[3] soot clustering,[4] protein accumulations,[5] wastewater treatment,[6] and marine aggregate formation in the oceans.[7,8] In all these cases, smaller particles move, at least in part, in an effectively random manner and may aggregate upon encountering other similar particles. The progressively larger aggregates thus formed often exhibit fractal structures.[1−8]

Arguably, the most effective and influential models of aggregation have been the diffusion-limited-aggregation (DLA) and diffusion-limited-cluster-aggregation (DLCA) models. In the DLA model,[9] individual particles undergo stochastic motion until they encounter a cluster that they then stick to, whereas in the DLCA model,[10,11] many particles move simultaneously, form clusters when encountering each other, and continue moving stochastically as clusters. These irreversible aggregation models focus on the initial stages of aggregation assuming that the lifetime of the bonding is much longer than the time scale of those initial stages.[12] Despite its simplified form of attractive interactions, the DLCA model has been successfully used to reproduce the characteristic features of the initial stages of aggregation. This is attributed to the observation that those features are not significantly influenced by the exact shape of the interparticle potential. In fact, from comparisons with more realistic reversible aggregation models, it was shown that, if the interactions are sufficiently strong, the structures obtained from those models approach the limit of irreversible DLCA.[13,14]

In most cases, the rationale for the stochastic motion of the particles is that they are subject to large numbers of molecular collisions. The effect of these collisions can be modeled as random forces in Langevin dynamics models or directly as random displacements in Brownian dynamics models.[15] The translational diffusivity of individual particles is well known to be inversely proportional to their size, as captured by the Stokes−Einstein relation.[16] As aggregates grow in size, the resistance of the surrounding fluid increases and aggregates are therefore expected to move slower than individual particles. This effect was studied early on in two-[17,18] and three-dimensional systems[19] but has been neglected in many DLCA studies. Furthermore, until recently, it was not clear how to determine the hydrodynamic radius of a fractal aggregate in a manner consistent with the Stokes−Einstein relation. A recent study[20] showed that the radius of gyration of an aggregate is an appropriate measure of its size. We study here the effects on the aggregation of having size-dependent diffusivities, following and extending the works of refs 17 and 19.

Early DLA models, where the particles were modeled as spheres and the aggregates formed were fixed, did not include the effects of particle rotation. However, once clusters are allowed to move stochastically, they are expected to rotate as

Received: June 7, 2022
Accepted: September 26, 2022
Published: October 31, 2022

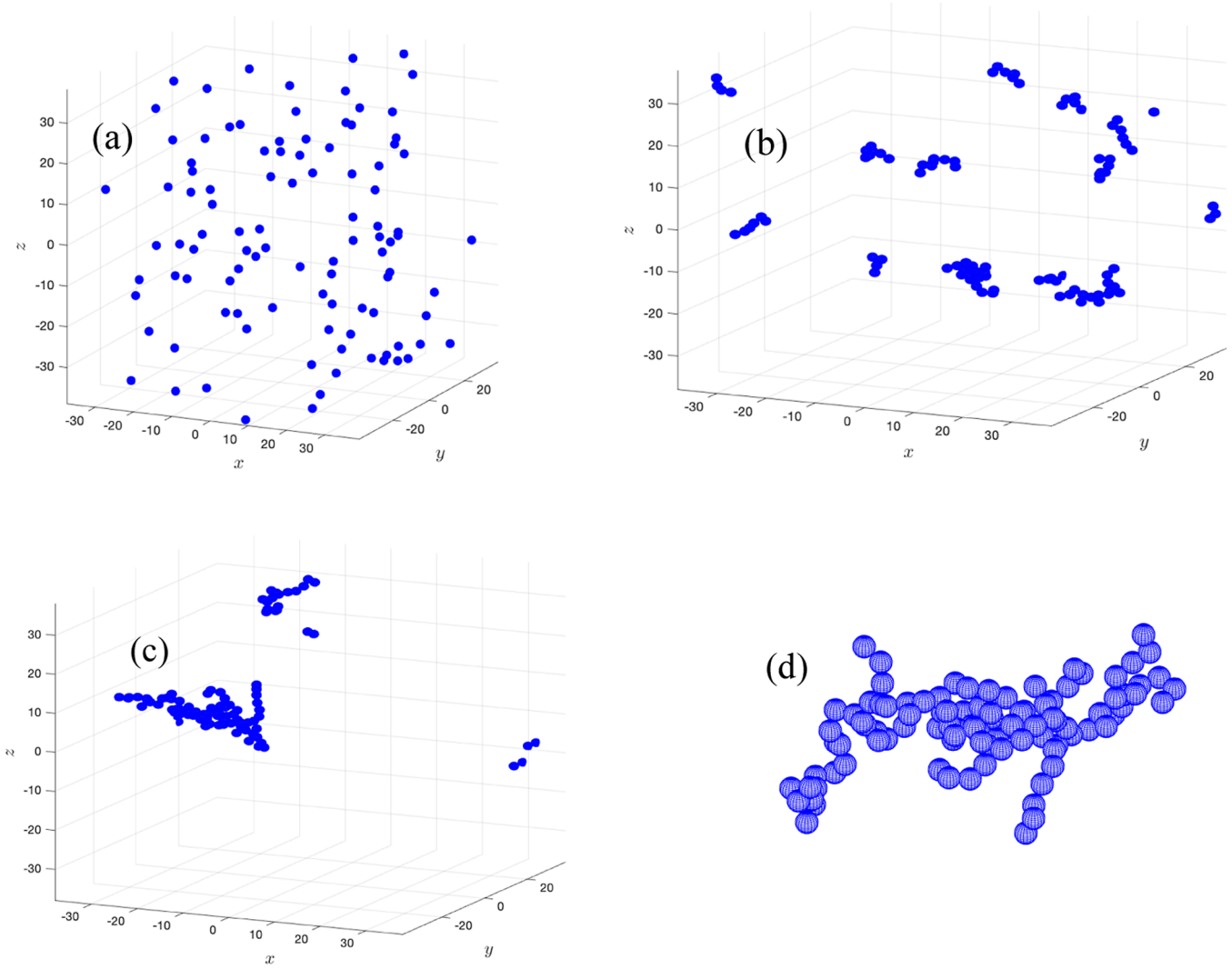

Figure 1. Time snapshots of a typical system with $N = 100$ spheres at time $t = 0$ in panel (a), $t = 200$ in panel (b), and $t = 1200$ in panel (c). Eventually, a single aggregate containing $M = 100$ spheres remains, as shown from a closer perspective in panel (d).

they are subjected to random torques as well. While early two-dimensional studies of DLCA incorporated the effects of rotation,[21] these effects were only recently taken into consideration in three-dimensional systems by Jungblut et al.[22] In contradiction to the prior assumption that the effects of rotation on aggregation would be negligible, they demonstrated that the rotation of clusters significantly alter the structure of the resulting aggregates. However, this conclusion was drawn by using constant rotational diffusivity. As indicated by the Stokes−Einstein−Debye relation,[23] the rotational diffusivity of an object is inversely proportional to the cube of its size, which, for aggregates, was shown to be well captured by the radius of gyration.[20] Based on these physical observations, we revisit here the effects of rotation. To this end, we present a DLCA model that incorporates rotational effects into Brownian dynamics and accounts, to the best of our knowledge for the first time, for the size dependence of the rotational diffusivity.

Another factor that can affect the dynamics of particles and clusters during the aggregation process is the density difference between the particles and the surrounding fluid. In many instances, particles, such as soot, plankton, or metal atoms, are denser than the surrounding medium. The gravitational acceleration will therefore cause particles to settle downward at a speed that increases with their size.[20,24−26] While this effect has been well quantified for aggregates already formed, to the best of our knowledge, it has not been incorporated in three-dimensional DLCA models. We therefore also study here the influence of a size-dependent settling velocity on the formation of aggregates.

The quantity typically used to characterize the fractal structures of randomly formed aggregates is their fractal dimension.[27] Models of DLCA (see for instance ref 28) as well as experiments[29,30] have reported fractal dimensions in the 1.7−1.8 range. However, lower fractal dimensions (1.5−1.6) have also been measured in soot aggregates[4] and a broad range of fractal dimensions (1.28−1.86) have been measured in marine aggregates.[31] In addition, models incorporating rotation[21,22,32] have reported fractal dimensions in the 1.5−1.6 range.

In this article, we discuss the impact of size-dependent diffusivities, rotation, and settling on the fractal dimension of aggregates formed via Brownian dynamics. In addition, we characterize the formation dynamics of the objects by comparing the growth in size of aggregates formed in various conditions. An aggregate's growth rate is an important and

https://doi.org/10.1021/acsomega.2c03547
ACS Omega 2022, 7, 40826−40835

under studied consideration, for example, for marine aggregates subject to competing dynamics such as biological activity as they aggregate.

The structure of the rest of this paper is as follows. In Section 2 we provide the details of our numerical simulations of aggregation via the Brownian motion of particles subject to size-dependent translational and rotational diffusion, as well as settling. In Section 3, we show and discuss our results regarding the growth rate of these aggregates and their fractal dimensions. We present our conclusions in Section 4.

2. METHODS

In our model, aggregates are built from identical spheres. We consider spheres of radius $R_1' \approx 1\ \mu$m or smaller, so that inertial effects are negligible. Brownian dynamics are applied to aggregates to randomly translate and rotate them.[15] In addition, following the DLCA model,[28] if any two spheres overlap (i.e., their centers of mass are within one sphere diameter), the aggregates containing them are made to merge irreversibly and move as a single aggregate thereafter. Hence, as time progresses, spheres merge into aggregates of various sizes and eventually form a single large aggregate. Snapshots taken from a typical simulation of our model are shown in Figure 1a−c, and the structure of the final aggregate obtained is shown in Figure 1d. We provide details of our model in the paragraphs below and in the Supporting Information.

We non-dimensionalize our system using the radius of a single sphere, R_1', as our characteristic length scale and using a diffusive time scale, $\tau' = (R_1')^2/2D_1'$, as our characteristic time scale, where D_1' is the translational diffusivity of a single sphere. Here, primes indicate dimensional quantities. In this setting, the dimensionless radius and translational diffusivity of a single sphere therefore become, respectively, $R_1 = 1$ and $D_1 = D_1'/((R_1')^2/\tau') = 0.5$.

We assume that aggregates have random structures but are roughly isometric so that their translational and rotational random motions can be described via corresponding scalar diffusion coefficients (as opposed to diffusion tensors). At each time step, spheres and aggregates are translated by $\Delta\vec{x} = \sqrt{2D\Delta t}\,\vec{\mathcal{N}}(0,1)$, where D is the translational diffusivity of an aggregate, Δt is the time step size, and $\vec{\mathcal{N}}(0,1)$ denotes a three-dimensional vector with independent random components drawn from the standard normal distribution (i.e., with zero mean and unit variance). To implement Brownian rotation, another random vector, $\Delta\vec{\theta} = \sqrt{2D_\theta\Delta t}\,\vec{\mathcal{N}}_\theta(0,1)$, is sampled, where D_θ is the rotational diffusivity of an aggregate and $\vec{\mathcal{N}}_\theta(0,1)$ is a three-dimensional random vector sampled similarly to $\vec{\mathcal{N}}(0,1)$. We compute the magnitude, $\Delta\psi = \|\Delta\vec{\theta}\|$, and unit vector, $\hat{\Theta} = \Delta\vec{\theta}/\|\Delta\vec{\theta}\|$, corresponding to this random vector. We then implement a rotation of angle $\Delta\psi$ about the axis $\hat{\Theta}$. A detailed description of the implementation of translational and rotational Brownian dynamics is given in Sections S1.3−S1.4 of the Supporting Information.

To build a more realistic model of aggregation, we allow diffusivities to be size dependent, as was previously done for translational diffusivity.[19] It has been shown[20] that the best length scale to describe the hydrodynamic resistance of fractal aggregates is the radius of gyration, R_g, and it was found that the translational and rotational friction coefficients of an aggregate are proportional to R_g and R_g^3, respectively. Because the corresponding diffusivities are inversely proportional to the friction coefficients, D and D_θ are proportional to $1/R_g$ and $1/R_g^3$, respectively, which is consistent with the Stokes−Einstein[16] and Stokes−Einstein−Debye equations[23] for the diffusivities of a sphere. For an aggregate made of M spheres of uniform density, the radius of gyration is defined as

$$R_g = \sqrt{\frac{3}{5} + \frac{1}{M}\sum_{m=1}^{M} \|\vec{x}_m - \vec{x}_c\|^2} \tag{1}$$

Here, $\vec{x}_m$ denotes the position of the mth sphere in the aggregate and $\vec{x}_c$ is the center of mass of the aggregate. Note that the definition of R_g for point-mass particles is slightly modified by the addition of 3/5 to accurately account for the non-zero radius of the spheres, which also recovers the radius of gyration of a single unit sphere with uniform mass distribution: $R_{g1} = \sqrt{3/5}$. From the Stokes−Einstein[16] and Stokes−Einstein−Debye[23] equations, the translational and rotational diffusivities for single spheres are set to $D = 0.5$ and $D_\theta = 0.375$, respectively. Using the results of Yoo et al.[20] on the friction coefficients of aggregates, the size-dependent diffusivities of aggregates are defined as

$$D = \frac{0.5}{R_g}, \text{ and } D_\theta = \frac{0.375}{R_g^3} \tag{2}$$

Further details on the relevant equations and their derivation are provided in Section S1.6 of the Supporting Information.

We aim to characterize the impact of size-dependent diffusivities and rotation on the structure of aggregates and their growth dynamics. To this end, we study four different cases:

- Case 1: $D = 0.5$, $D_\theta = 0$,
- Case 2: $D = 0.5$, $D_\theta = 0.375$,
- Case 3: $D = 0.5/R_g$, $D_\theta = 0$,
- Case 4: $D = 0.5/R_g$, $D_\theta = 0.375/R_g^3$.

In Case 1, we follow the traditional DLCA approach, see for instance ref 28, where rotational diffusion is not incorporated and translational diffusivity is kept constant. In Case 2, we incorporate rotation, keeping diffusivities constant, as in ref 22. In Case 3, while rotation is absent, we allow translational diffusivity to be size-dependent, similarly to ref 19. In Case 4, we use more realistic size-dependent diffusivities for both translation and rotation. To the best of our knowledge, the latter model has not been studied to date.

When spheres have a greater density than the surrounding fluid, they will, in addition to being subject to Brownian dynamics, settle under the influence of gravity. While this effect was neglected up to this point as it is often small, it is more likely to become influential for larger aggregates. We therefore study Case 5, with the same conditions as Case 4 supplemented by a size-dependent aggregate settling speed, U, which is determined by balancing the weight and the drag force as characterized by their radius of gyration.[20] For aggregates containing M spheres and with radius of gyration R_g, one finds that

$$U = \Gamma\frac{M}{R_g} \tag{3}$$

where Γ is the dimensionless gravitational potential energy of a single sphere and is proportional to the density difference between the spheres and the surrounding fluid and to $(R_1')^4$, as

https://doi.org/10.1021/acsomega.2c03547
ACS Omega 2022, 7, 40826−40835

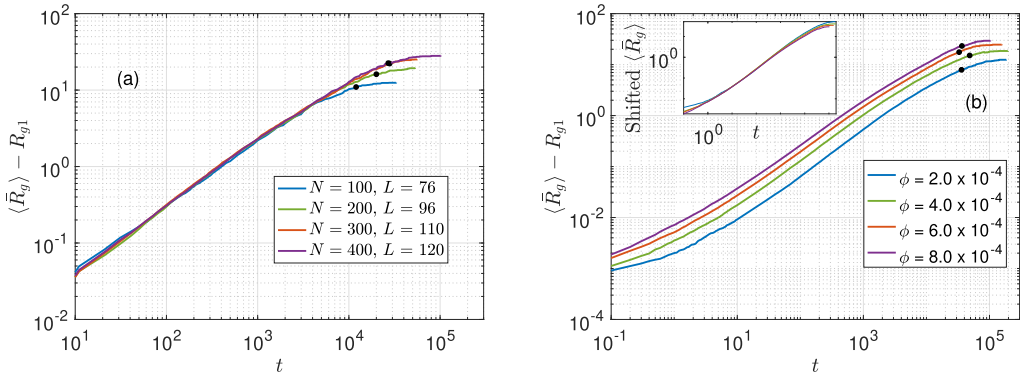

Figure 2. Growth over time of the average radius of gyration of aggregates, $\langle \bar{R}_g \rangle$, relative to their initial value, R_{g1}, for Case 4. Panel (a) compares the results obtained for a fixed volume fraction $\phi = 10^{-3}$ and different system sizes (specified by the total number N of spheres and the different domain side lengths L). Panel (b) compares the results of different volume fractions ϕ for a fixed system size with side length $L = 128$. On each curve, t_{max} is shown as a black dot. The inset shows the same curves superimposed by vertical translation.

detailed in Section S1.7 of the Supporting Information. We consider three different sets of parameters, denoted by Cases 5a, 5b, and 5c. In these cases, single spheres are computed to have settling speeds of, respectively, $U_1 = 0.525$, 1.05, and 2.10, while aggregates containing M spheres have $\Gamma = 0.55$, 1.10, and 2.20 for a settling speed of

$$U = 0.55\frac{M}{R_g} \text{ (Case 5a)},$$
$$U = 1.10\frac{M}{R_g} \text{ (Case 5b)},$$
$$U = 2.20\frac{M}{R_g} \text{ (Case 5c)} \quad (4)$$

In our simulations, the ratio M/R_g is typically of order one and does not exceed 20. We note that a size-dependent aggregate Péclet number is found to be $Pe = U'R_g'/D' = 2\Gamma R_g M$. This indicates that whenever settling is present its importance grows very quickly with aggregate sizes, as both M and R_g grow, with a magnitude prescribed by the dimensionless gravitational potential energy of a single sphere Γ.

In our Brownian dynamics simulations for Case 5, the settling velocity is implemented as a bias in the vertical direction, which is added to Case 4. Details of the parameter selection, computation, and implementation of the settling speed in Brownian dynamics are given in Section S1.7 of the Supporting Information.

For all cases considered in our simulations, we initially confine single spheres to a cubic box of side length $L = 128$ (unless otherwise stated) with periodic boundary conditions applied in all directions. The time step size Δt is chosen to be small enough to ensure that the overlap between adjacent spheres never exceeds 5% of their total volume. This corresponds to setting $\Delta t = 0.01$ in all cases, except when rotational diffusion is constant (Case 2) and large aggregates are present, when Δt was chosen to be as small as $\Delta t = 0.001$. The total number of speres N is varied between 100 and 400, giving a range of volume fraction $\phi = (4/3)\pi N/L^3$ between 2×10^{-4} and 10^{-3}. Unless otherwise stated, we collect a total of 400 samples per volume fraction for each case under study. We provide further details on the validation of our implementation in Section S2.1, on the selection of the time step size in Section S2.2, and on our data collection method in Section S2.4 of the Supporting Information.

We monitor over time the radius of gyration R_g of the aggregates as well as the number of spheres M they contain. To characterize the dynamical evolution of the aggregates, we introduce a weighted average of the radius of gyration within a system

$$\bar{R}_g = \frac{1}{N}\sum_{n=1}^{N} R_g^{(n)} \quad (5)$$

where $R_g^{(n)}$ denotes the radius of gyration of the aggregate containing the nth sphere. We note that $\bar{R}_g$ is computed from each sample as a function of time and that in this average, aggregates with a large number of spheres, M, will have a larger weight, as their radius of gyration is summed M times. We then take the average of $\bar{R}_g$ over all samples formed in the same conditions, which we denote $\langle \bar{R}_g \rangle$.

3. RESULTS AND DISCUSSION

3.1. Growth Rate. We investigate the size growth of aggregates over time using the weighted average of the radius of gyration $\langle \bar{R}_g \rangle$ and compare the results of Cases 1−4 to discuss the effects of size-dependent diffusivities as well as rotation. Before comparing those results, we first report the effects of finite system-size on the time profile of $\langle \bar{R}_g \rangle$ and also investigate the dependence of the latter quantity on the volume fraction ϕ to justify our choice of simulation parameter values. We note that contrary to molecular dynamics simulation models, whose finite system-size effects have been well understood (see, e.g., refs 33 and 34), these effects have not been as systematically investigated for aggregation models.

We show in Figure 2a the time profiles of the average radius of gyration of aggregates obtained from 36 samples in Case 4 for different domain sizes, L, and a fixed volume fraction $\phi = 10^{-3}$. For reference, we note that $\langle \bar{R}_g \rangle = R_{g1}$ at $t = 0$ and that if two spheres meet and form an aggregate the increase in radius of gyration is approximately 0.5. We observe that there is a time period where the growth of $\langle \bar{R}_g \rangle$ is independent of L and is well described by a power law (i.e., a straight line in the log−log plot). At later times, the number of spheres available for aggregation decreases and eventually the growth saturates as

https://doi.org/10.1021/acsomega.2c03547
ACS Omega 2022, 7, 40826−40835

too few spheres remain to maintain growth. This behavior happens later for larger domains as they initially contain more spheres. We will focus our study on the time period before saturation occurs, that is, $t \leq t_{max}$, where we define t_{max} as the first time when the slope of the growth rate of the radius of gyration in the log−log scales (as shown in Figure 2) becomes less than half what it was over the time period where it remained approximately constant. More details about the definition of t_{max} can be found in Section S2.4 of the Supporting Information.

We also investigate aggregate growth for various volume fractions and for a fixed domain size, $L = 128$, as shown in Figure 2b. We see that the very early growth for $t \lesssim 1$ is faster for larger volume fractions. This is a reflection of the higher probability that two spheres have initial positions that are separated by a very short distance when the volume fraction is larger. Less time is then required for spheres to first encounter each other. However, the increase in $\langle \overline{R}_g \rangle$ during this time period is rather small ($<10^{-2}$). More significantly, in a wide time range for $t > 1$ and before finite-size effects start impacting the results, all curves can be superimposed by vertical translation, as shown in the inset of Figure 2b. This indicates that the slopes of the curves in the log−log scales are independent of the volume fraction ϕ. Thus, in a time period where the curves exhibit a nearly constant slope, the growth over the time period can be characterized by an exponent α in the following relation

$$\langle \overline{R}_g \rangle = C(\phi) t^{\alpha} + R_{g1} \tag{6}$$

The values of α estimated in Cases 1, 3, and 4 are given in Table 1. The time range used for linear regression was between the time t_1 for which $\langle \overline{R}_g(t_1) \rangle - R_{g1} = 1$ and t_{max}. For all cases, corresponding plots to Figure 2b are given in Section S3.1 of the Supporting Information. Overall similar trends are observed for Cases 1−4 except that an acceleration in growth appears before saturation in Case 2, as discussed below.

Table 1. Values of the Exponent α and the Fractal Dimension d for Cases 1−4

	diffusivities	exponent α[a]	fractal dimension d[b]
Case 1	$D = 0.5, D_\theta = 0$	1.02	1.82 ± 0.02
Case 2	$D = 0.5, D_\theta = 0.375$	not applicable	1.23 ± 0.10
Case 3	$D = 0.5/R_g, D_\theta = 0$	0.66	1.81 ± 0.02
Case 4	$D = 0.5/R_g, D_\theta = 0.375/R_g^3$	0.71	1.69 ± 0.01

[a]See eq 6 for mathematical definition and Figure 3 for actual estimation. [b]See eq 7 for mathematical definition and Figure 4 for actual estimation.

As shown in Figure 2b, at $t = 10$ the aggregates' average radius of gyration has grown by less than 0.1, showing that most spheres have yet to encounter other spheres. Rotational effects and size-dependent diffusivities thus have a negligible effect on the growth of the aggregates up to that time. At the other end of the spectrum, after t_{max} the growth of the aggregates slows down and saturates, as too few spheres remain to maintain growth. Therefore, we focus on the effects of rotational diffusion and size-dependent diffusivity on aggregate growth over the time interval $10 \leq t \leq t_{max}$, where the volume fraction of spheres has only a negligible effect. We show in Figure 3 the temporal evolution of the average size of

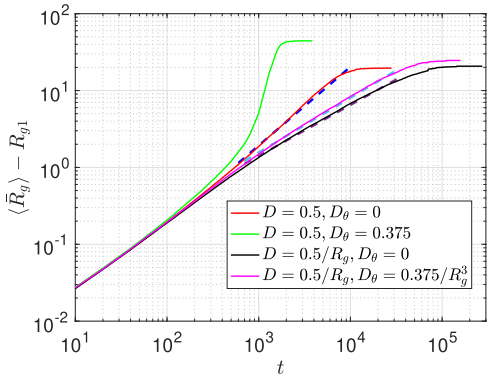

Figure 3. Comparison of the growth patterns of average radius of gyration observed in Cases 1−4 for volume fraction $\phi = 6 \times 10^{-4}$. The time profiles of $\langle \overline{R}_g \rangle - R_{g1}$ are shown in the log−log scales as solid lines. For each case except Case 2, linear regressions are also shown as dashed lines. In each case, the time range $[t_1, t_2]$ for linear regression was chosen such that $\langle \overline{R}_g(t_1) \rangle - R_{g1} = 1$ and $t_2 = t_{max}$.

aggregates for $\phi = 6 \times 10^{-4}$ for Cases 1−4. For $t < 100$, the four curves overlap, indicating that, at those early times, aggregates exhibit the same growth dynamics. In this regime, the size dependence of the diffusivities is still weak, as most aggregates are still small, and aggregates move as if their diffusivities were constant. Moreover, rotational diffusion has no effect on single spheres, which still constitute most of the aggregates.

As time increases past $t = 100$, differences in the four cases emerge. Unsurprisingly, when the diffusivities are reduced with aggregate size, the growth slows. In the absence of rotation, we see that Case 3 produces a slower growth than Case 1 and similarly Case 4 produces a slower growth than Case 2, which has constant non-zero diffusivities for both translation and rotation. In the latter case (green curve), the growth of the aggregates accelerates as time progresses and becomes faster than a power law. This is due to the larger displacements induced by a fixed rotational diffusivity applied to larger aggregates. In fact, this is the only case where we had to reduce the simulation time step size, using values as low as $\Delta t = 0.001$ to limit the magnitude of those displacements. Such larger displacements clearly facilitate aggregation, yielding much faster growth. However, it is unlikely that real aggregates can maintain a constant rotational diffusivity as they grow because the resistance of the surrounding fluid to rotation typically grows with the cube of the aggregate size.[20]

The second fastest growth, which exhibits a power-law behavior throughout, is observed to be the classic DLCA with fixed translational diffusivity and without rotation (Case 1, red curve). In this case, the growth is nearly linear in time, with a best fit yielding $\langle \overline{R}_g \rangle = C_1(\phi) t^{1.02} + R_{g1}$.

In the two cases, where diffusivities are size-dependent, whether rotation is absent (Case 3, black curve) or present (Case 4, magenta curve), the growth is quite similar and appears to follow a power law but is markedly slower than for DLCA. The presence of rotation again is observed to accelerate growth, as it provides an additional displacement, which increases the odds of coming into contact with another aggregate. However, because of the strong dependence of D_θ on R_g, this effect remains small. The growth rate therefore appears to be mostly set by the translational diffusivities. Best fits of the growth rates are found to be

https://doi.org/10.1021/acsomega.2c03547
ACS Omega 2022, 7, 40826−40835

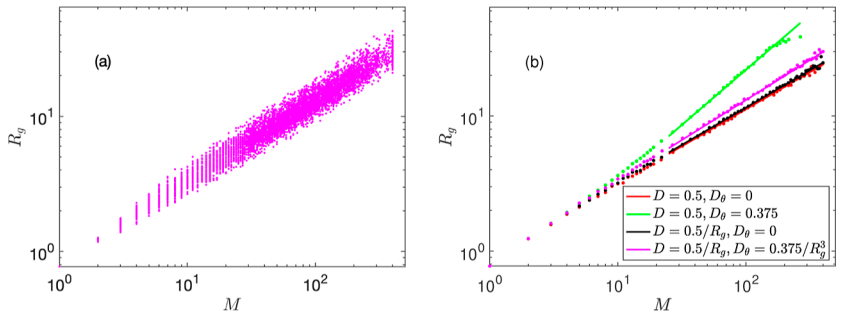

Figure 4. Radius of gyration, R_g, of aggregates observed at time t_{max} as a function of the number of spheres in an aggregate, M. Panel (a) shows the scatter plot of R_g vs M for Case 4 for all volume fractions on a log−log scale. Panel (b) compares the results of Cases 1−4 for all volume fractions, where, for visual clarity, each dot represents the average value of R_g computed over a small interval around a given value of M. The corresponding scatter plot of each case is shown in Section S3.2 of the Supporting Information. Solid lines depict the linear regression results based on data for which $M \geq 25$. For Case 2 (green line), aggregates of maximum radius greater than or equal to half the domain size were discarded.

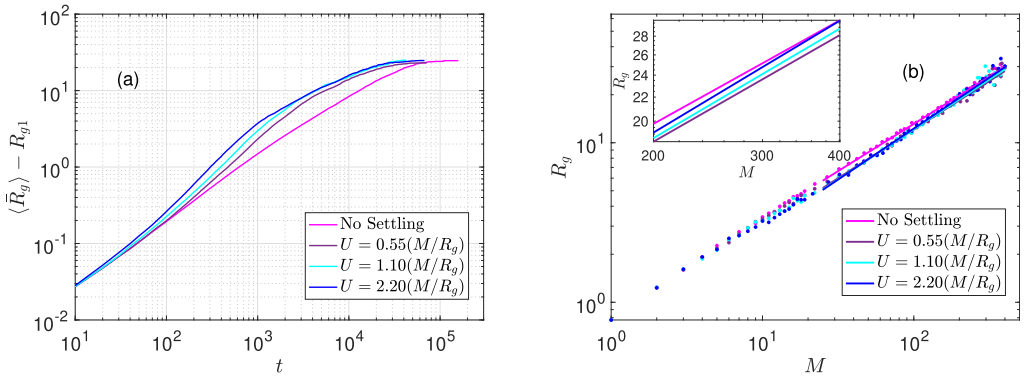

Figure 5. Comparison of simulation results without settling (Case 4: magenta) and with size-dependent settling for different values of Γ (Cases 5a: purple, 5b: cyan, and 5c: blue). Size-dependent diffusivities are used in all four cases. Panel (a) shows the time profiles of $\langle \bar{R}_g \rangle - R_{g1}$ in the log−log scales for volume fraction $\phi = 6 \times 10^{-4}$. Panel (b) compares the results of Cases 4, and 5a−5c for all volume fractions, where, for visual clarity, each dot represents the average value of R_g computed over a small interval around a given value of M. The corresponding scatter plot of each case is shown in Section S3.2 of the Supporting Information. Solid lines depict the linear regression results based on data for which $M \geq 25$. The inset shows only the fitted lines for the range $M \geq 200$ to emphasize where they differ.

$\langle \bar{R}_g \rangle = C_3(\phi)t^{0.66} + R_{g1}$ in the absence of rotation (Case 3) and $\langle \bar{R}_g \rangle = C_4(\phi)t^{0.71} + R_{g1}$ for the most complete model (Case 4) that includes both rotation and size-dependence. Note that while the prefactors in the above relationships depend on ϕ, the powers of t found are consistent across all the volume fractions analyzed.

3.2. Fractal Dimension. We now wish to characterize the structure of aggregates observed in the course of aggregation. In general, they are fractal objects with a dimension between one and two, meaning that they are denser than one-dimensional chains but less compact than two-dimensional sheets. For example, if we look at the number of nearest neighbors of a sphere that is part of an aggregate, we find that a majority of spheres have the two nearest neighbors, as in linear objects. About 25% of spheres have only one neighbor, forming the end of a branch, and roughly the same number of spheres have three or more nearest neighbors, as they would in a two-dimensional object. This is illustrated in more detail in Section S2.3 of the Supporting Information. More precisely, we can characterize the aggregates in terms of their fractal dimension, d. To this end, we use the well-known relationship[19,28] between the number of spheres M in an aggregate and its size, here characterized by the radius of gyration R_g

$$R_g \sim M^\beta, \text{ with } \beta = \frac{1}{d} \tag{7}$$

As shown in Figure 4a for Case 4, R_g grows approximately as a power of M, with that power being the inverse of the fractal dimension, consistent with eq 7. As shown in Section S3.2 of the Supporting Information, Cases 1 and 3 yield a similar relationship, as does Case 2 (with constant rotational diffusivity and exhibiting the fastest growth), with the caveat that in that case the size of the largest aggregates eventually becomes limited by the domain size.

To find d, we apply eq 7 to data collected at time t_{max}. We focus on aggregates of size $M \geq 25$ to ensure that we are looking at fractal-like objects. Figure 4b shows a linear fit of the radius of gyration as a function of M for Cases 1−4, and the fractal dimensions found are listed in Table 1. Because the choice of the range of M values for linear regression may affect the resulting estimated value of d, we also compute linear regressions using two different ranges, $M \geq 5$ and $M \geq 50$, and use them to quantify the level of uncertainty in the d values.

Our results for cases without rotation, Cases 1 and 3, are consistent with previous numerical simulations of DLCA, for example, refs 19 and 28. However, including rotational diffusion lowers the fractal dimension of the aggregates, most significantly when it is constant. This can be understood by noting that larger aggregates subject to rotation will have their

https://doi.org/10.1021/acsomega.2c03547
ACS Omega 2022, 7, 40826−40835

tips experience the largest displacements. This in turn increases the probability that contact with surrounding aggregates will take place at or near the tips, resulting in an object with a more linear structure and therefore a smaller fractal dimension.

The trend of rotational diffusion lowering fractal dimension was previously reported in two-dimensional simulations[18,21] as well as a recent simulation study with a setup similar to Case 2 with a constant rotational diffusivity by Jungblut et al..[22] In the latter study, using Langevin dynamics rather than Brownian dynamics and considering systems of a volume fraction approximately 10 times greater than ours, a value of fractal dimension of 1.55 ± 0.02 was reported, which is greater than what was found in the present study. We note that this fractal dimension was obtained using data for both smaller aggregates than what was used here and considering aggregates that had reached the percolation limit, where an aggregate can connect with itself via the periodic boundary conditions, both of which tend to increase the computed fractal dimension.

As can be seen comparing Cases 1 and 3, incorporating a size-dependent translational diffusivity is found to cause only a very small reduction of the fractal dimension. The aggregates' structure then appears to remain qualitatively the same and to simply be formed slower when D is size-dependent. Finally, the model with both rotation and size-dependent diffusivities, Case 4, shows a slightly reduced fractal dimension, $d = 1.69$, compared to DLCA. This is most likely due to the inclusion of rotational diffusion, which generates less compact aggregates. However, taking into account the size dependence of the rotational diffusion greatly reduces this effect. The ratio of the diffusivities, $D/D_\theta = (4/3)R_g^2$, indicates that as the aggregates become larger, translational diffusion becomes dominant, and the resulting aggregates are closer in structure to those formed by DLCA.

3.3. Settling. We present in this section results for Cases 5a−5c, where settling is added to Case 4 using a different value of the single sphere gravitational potential energy Γ in each case. From equations 4 and 7, we see that for $d > 1$, the settling speed of an aggregate increases with its size, potentially affecting the formation dynamics of aggregates and their resulting structure. Note that for Cases 5a−5c, results presented were obtained from 100 samples. Figure 5a shows that, at early times, incorporating settling in the simulations does not have a significant effect on the growth of aggregates. This is because settling affects dynamics when aggregates have different settling speeds, which only happens when a range of aggregate sizes is present. However, in the time range $40 < t < 100$, the growth of the aggregates is accelerated by the presence of settling, and it can readily be seen that increasing the value of Γ enhances this effect. This acceleration is attributable to larger aggregates settling faster and effectively capturing smaller aggregates located in a vertical column beneath them as they settle. We note that this process takes place over a settling time scale, which here is significantly faster than the diffusive time scale. As a result, finite system-size effects can be felt earlier than in the absence of settling. In other words, in a periodic domain, larger aggregates can quickly collect all smaller aggregates within their vertical column and then continue to grow slowly due to horizontal diffusive effects. More care to avoid system-size effects must therefore be taken in simulations of aggregation that include settling.

As can be seen in Figure 5b and in the values listed in Table 2, the fractal dimension of aggregates formed in the presence of settling decreases as the importance of settling, characterized by the gravitational potential energy of a single sphere Γ, increases. For the largest effect of settling we considered, $\Gamma = 2.20$, we find a fractal dimension of $d = 1.56 \pm 0.06$. Moreover, settling breaks the isotropy of the system and distinguishes the vertical direction (denoted with coordinate z) from the horizontal directions (denoted with coordinates x and y). To quantify the effect of this break in symmetry, we measure coordinate specific components of the radius of gyration for Cases 5a−5c. We define the vertical component of the radius of gyration of an aggregate as

$$R_z = \sqrt{\frac{1}{M}\sum_{m=1}^{M}(z_m - z_c)^2} \tag{8}$$

and we define R_x and R_y analogously. Figure 6 compares the scatter plot of R_y versus R_x with that of R_z versus R_x at $t = 4000$ from 100 samples for $\phi = 8 \times 10^{-4}$ for Case 5b, with Cases 5a and 5c exhibiting similar results. The best fits, obtained by averaging the polar angle of the data plotted, are, respectively, $R_y = 0.99R_x$ and $R_z = 0.92R_x$. This indicates that, as a statistical average, the size of an aggregate in the x and y directions is effectively the same, but that aggregates are on average smaller in the vertical direction.

Even in the absence of settling, individual aggregates do not generally have the same extent in every direction. However, the direction in which they are the shortest is then uniformly distributed. In the presence of settling, the shortest direction is statistically preferentially aligned with the vertical. We define the average aggregate aspect ratio γ using the best fit of R_z versus R_x as

$$R_z = \gamma R_x \tag{9}$$

and compute it also for Cases 5a and 5c. The results are summarized in Table 2. While this aspect ratio remains close to one, it nonetheless reflects the influence of the settling direction on the structure of the aggregates formed and shows that the anisotropy increases with the magnitude of the settling speed. We note that, at earlier times, a smaller difference between the horizontal and vertical directions is observed, presumably because the effects of settling are not yet at their peak. At later times, the vertical extent is also observed to be closer to the horizontal extent. We suspect that finite system-size effects then come into play in this behavior as settling first depletes available aggregates in vertical columns and further growth effectively occurs sufficiently slowly through horizontal diffusive processes to allow rotational diffusion to re-orient aggregates in an isotropic manner. When the departure from statistical isotropy becomes significant, the assumption of

Table 2. Values of the Fractal Dimension d for Cases 4 and 5a−5c

	single sphere Grav. P.E. Γ^a	fractal dimension d^b	aspect ratio γ^c
Case 4	0.0	1.69 ± 0.01	0.99
Case 5a	0.55	1.64 ± 0.08	0.94
Case 5b	1.10	1.60 ± 0.07	0.92
Case 5c	2.20	1.56 ± 0.06	0.90

[a]See eq 3 for relation between Γ and settling speed U and eq 22 of the Supporting Information for its definition. [b]See eq 7 for mathematical definition and Figure 5b for actual estimation. [c]See eq 9 for mathematical definition.

https://doi.org/10.1021/acsomega.2c03547
ACS Omega 2022, 7, 40826−40835

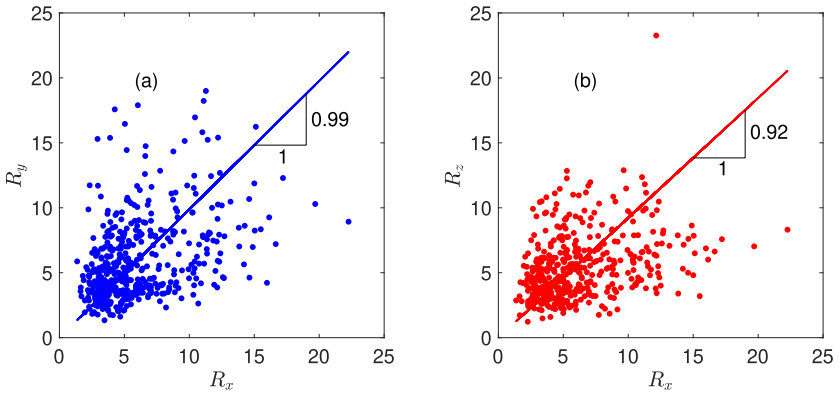

Figure 6. Evidence of anisotropy in aggregates formed in the presence of settling, for $\Gamma = 1.10$ (Case 5b). Here, the quantities R_η ($\eta = x, y,$ or z) represent the contribution of each direction η to the radius of gyration of an aggregate, see eq 8. Panel (a) shows a scatter plot of R_y vs R_x and panel (b) shows a scatter plot of R_z vs R_x. The solid lines are the best fitted line obtained by averaging the polar angle of the data points and are of slope 0.99 for panel (a) and 0.92 for panel (b). Simulation results were collected at $t = 4000$ for $\phi = 8 \times 10^{-4}$ from 100 samples.

scalar diffusivities is no longer appropriate and diffusivity tensors must be used to describe the Brownian motion of each aggregate.[35,36] This will be an important consideration to incorporate in future simulations where settling effects are dominant.

4. CONCLUSIONS

In this paper, we studied the impact of size-dependent diffusivities and rotation on the formation mechanisms of aggregates. To this end, we investigated the growth rate and fractal dimension of aggregates by computing the radius of gyration R_g over time. To ensure that the conclusions of our simulation study be independent of the size of the simulation domain, we systematically investigated the finite system-size effects on these quantities. We considered a dilute regime, where the solid volume fraction, was seen to only be impactful in the very early stages of aggregation.

We found that including size-dependent translational diffusivity, D, into the traditional DLCA model has a negligible impact on the fractal dimension, d, of the aggregates formed, which remained near $d = 1.8$. However, we observed that a size-dependent D significantly reduces the growth rate of aggregates, with their average radius of gyration growing like $\langle \overline{R}_g \rangle \sim t^{0.66}$ compared to $\langle \overline{R}_g \rangle \sim t^{1.02}$ in DLCA.

The effects of non-zero rotational diffusion, D_θ, were found to be significant for a constant D_θ. The aggregates then grew much faster and had a significantly reduced fractal dimension, $d = 1.23$. However, this scenario is not appropriate to systems, where diffusive effects are due to molecular effects, as the rotational friction coefficient quickly increases with the aggregate size. The use of a more realistic, size-dependent, D_θ, greatly reduced the impact of rotational diffusion as larger aggregates rotated much more slowly owing to the $D_\theta \sim R_g^{-3}$ scaling. Nonetheless, the fractal dimension of aggregates formed with size-dependent D_θ was reduced compared to DLCA, yielding $d = 1.69$, and their growth rate was accelerated to scale as $\langle \overline{R}_g \rangle \sim t^{0.71}$.

To obtain even more realistic models of aggregation, we also included gravitational effects, causing the aggregates to settle at a rate depending on their size and on the choice of a dimensionless parameter here set to $\Gamma = 0.55, 1.10, 2.20$. We found that settling, much like rotational diffusion, hastened the growth of aggregates and resulted in aggregates of smaller fractal dimension, $d = 1.64, 1.60, 1.56$, for the parameters we considered. We also observed the breaking of isotropy in this case, resulting in aggregates with a slightly shorter vertical extent compared to their horizontal extent. Depending on the size and density of the aggregating spheres, the impact of settling can vary from negligible to dominant and a more systematic study of this effect remains to be completed. Our simulations revealed that finite system-size effects quickly come into play in the presence of settling, so that obtaining results applicable to larger systems likely require significantly greater computational effort.

In order to obtain a realistic model of aggregation, several other factors will eventually need to be taken into account. For example, particles may only stick to each other with a certain probability rather than automatically as we have assumed,[37] leading to a transition from DLCA to reaction-limited cluster aggregation (RLCA). It would be also interesting to consider a more realistic potential for the van der Waals interaction and investigate its effect. In many cases,[32,38] particles can become charged, leading to either attractive or repulsive interactions that can be modeled via the Derjaguin−Landau−Verwey−Overbeek (DLVO) theory. Hydrodynamic interactions can also affect the diffusivity of particles, particularly at a low Reynolds number and as the distance between particles becomes small. Such interactions break the isotropy of the system, and the scalar diffusivities describing the motion of each particle must be replaced by diffusivity tensors. Such tensors may be computed using accurate but computationally expensive methods such as multipole methods[39] or approximated focusing on nearest neighbors interactions using, for example, the Rotne−Prager−Yamakawa approximation[35,36] as has been done in bead models of macromolecular formation[40] and as was more generally reviewed in ref 41. Moreover, the suspending fluid itself may not be at rest, either moving in a deterministic manner in a rotating tank[42] or subject to turbulence. Such flows can affect the effective translational and rotational diffusivities of aggregates. In addition, aggregates are known to break up or disaggregate,[43,44] either under the effect of external flows or under the stress due to their own settling. Disaggregation is likely to modify the types of aggregates that may be collected; aggregates with the lowest fractal dimensions are most likely to break up and therefore will be less likely to be observed. The present work was a step toward making aggregation models more realistic by including

https://doi.org/10.1021/acsomega.2c03547
ACS Omega 2022, 7, 40826−40835

rotational diffusion and size-dependence and exploring the impact of settling. The features mentioned here underline that several more steps remain to be taken to obtain a complete model of aggregation.

■ ASSOCIATED CONTENT

Supporting Information

The Supporting Information is available free of charge at https://pubs.acs.org/doi/10.1021/acsomega.2c03547.

Detailed description of the model and its implementation; validation of the method, histograms for the overlapping volume and the number of nearest neighbors, and time range considered; complete data set for aggregate growth analysis; and fractal dimension computation (PDF)

■ AUTHOR INFORMATION

Corresponding Authors

Changho Kim − *Department of Applied Mathematics, University of California, Merced, California 95343, United States*; orcid.org/0000-0002-4064-8237; Email: ckim103@ucmerced.edu

François Blanchette − *Department of Applied Mathematics, University of California, Merced, California 95343, United States*; Email: fblanchette@ucmerced.edu

Author

Matteo Polimeno − *Department of Applied Mathematics, University of California, Merced, California 95343, United States*

Complete contact information is available at: https://pubs.acs.org/10.1021/acsomega.2c03547

Notes

The authors declare no competing financial interest.

■ ACKNOWLEDGMENTS

The authors acknowledge the support of the National Science Foundation Research and Training grant no. DMS-1840265.

■ REFERENCES

(1) Brady, R.; Ball, R. Fractal Growth of Copper Electrodeposits. *Nature* **1984**, *309*, 225−229.

(2) Argoul, F.; Arneodo, A.; Grasseau, G.; Swinney, H. L. Self-Similarity of Diffusion-Limited Aggregates and Electrodeposition Clusters. *Phys. Rev. Lett.* **1988**, *61*, 2558−2561.

(3) Ziegler, C.; Wolf, A.; Liu, W.; Herrmann, A.-K.; Gaponik, N.; Eychmüller, A. Modern Inorganic Aerogels. *Angew. Chem., Int. Ed.* **2017**, *56*, 13200−13221.

(4) Chakrabarty, R. K.; Moosmüller, H.; Arnott, W. P.; Garro, M. A.; Tian, G.; Slowik, J. G.; Cross, E. S.; Han, J.-H.; Davidovits, P.; Onasch, T. B.; Worsnop, D. R. Low Fractal Dimension Cluster-Dilute Soot Aggregates from a Premixed Flame. *Phys. Rev. Lett.* **2009**, *102*, 235504.

(5) Vreeker, R.; Hoekstra, L. L.; den Boer, D. C.; Agterof, W. G. M. Fractal Aggregation of Whey Proteins. *Food Hydrocolloids* **1992**, *6*, 423−435.

(6) Logan, B. E.; Wilkinson, D. B. Fractal Geometry of Marine Snow and Other Biological Aggregates. *Limnol. Oceanogr.* **1990**, *35*, 130−136.

(7) Alldredge, A. L.; Silver, M. W. Characteristics, Dynamics and Significance of Marine Snow. *Prog. Oceanogr.* **1988**, *20*, 41−82.

(8) Burd, A. B.; Jackson, G. A. Particle Aggregation. *Ann. Rev. Mar. Sci.* **2009**, *1*, 65−90.

(9) Witten, T. A.; Sander, L. M. Diffusion-Limited Aggregation, a Kinetic Critical Phenomenon. *Phys. Rev. Lett.* **1981**, *47*, 1400−1403.

(10) Kolb, M.; Botet, R.; Jullien, R. Scaling of Kinetically Growing Clusters. *Phys. Rev. Lett.* **1983**, *51*, 1123−1126.

(11) Meakin, P. Diffusion-Controlled Cluster Formation in 2−6-Dimensional Space. *Phys. Rev. A: At., Mol., Opt. Phys.* **1983**, *27*, 1495−1507.

(12) Jungblut, S.; Eychmüller, A.Modeling nanoparticle aggregation. *Chemical Modelling*; The Royal Society of Chemistry, 2019; Vol. *15*; pp 1−27.

(13) Lu, P. J.; Zaccarelli, E.; Ciulla, F.; Schofield, A. B.; Sciortino, F.; Weitz, D. A. Gelation of particles with short-range attraction. *Nature* **2008**, *453*, 499−503.

(14) Zaccarelli, E.; Lu, P. J.; Ciulla, F.; Weitz, D. A.; Sciortino, F. Gelation as arrested phase separation in short-ranged attractive colloid-polymer mixtures. *J. Phys.: Condens. Matter* **2008**, *20*, 494242.

(15) Bian, X.; Kim, C.; Karniadakis, G. E. 111 Years of Brownian Motion. *Soft Matter* **2016**, *12*, 6331.

(16) Einstein, A.*Investigations on the Theory of the Brownian Motion*; Dover: New York, 1956.

(17) Meakin, P. Formation of Fractal Clusters and Networks by Irreversible Diffusion-Limited Aggregation. *Phys. Rev. Lett.* **1983**, *51*, 1119−1122.

(18) Saffman, P. G.; Delbrück, M. Brownian Motion in Biological Membranes. *Proc. Natl. Acad. Sci. U.S.A.* **1975**, *72*, 3111−3113.

(19) Ansell, G. C.; Dickinson, E. Short-Range Structure of Simulated Colloidal Aggregates. *Phys. Rev. A: At., Mol., Opt. Phys.* **1987**, *35*, 2349−2352.

(20) Yoo, E.; Khatri, S.; Blanchette, F. Hydrodynamic Forces on Randomly Formed Marine Aggregates. *Phys. Rev. Fluids* **2020**, *5*, 044305.

(21) Meakin, P. The Effects of Rotational Diffusion on the Fractal Dimensionality of Structures Formed by Cluster−Cluster Aggregation. *J. Chem. Phys.* **1984**, *81*, 4637−4639.

(22) Jungblut, S.; Joswig, J.-O.; Eychmüller, A. Diffusion-Limited Cluster Aggregation: Impact of Rotational Diffusion. *J. Phys. Chem. C* **2019**, *123*, 950−954.

(23) Debye, P. J. W.*Polar Molecules*; Dover: New York, 1929.

(24) Wiltzius, P. Hydrodynamic Behavior of Fractal Aggregates. *Phys. Rev. Lett.* **1987**, *58*, 710−713.

(25) Johnson, C. P.; Li, X.; Logan, B. E. Settling Velocities of Fractal Aggregates. *Environ. Sci. Technol.* **1996**, *30*, 1911−1918.

(26) Takayasu, M. M.; Galembeck, F. Determination of the Equivalent Radii and Fractal Dimension of Polystyrene Latex Aggregates from Sedimentation Coefficients. *J. Colloid Interface Sci.* **1998**, *202*, 84−88.

(27) Sorensen, C. M. The Mobility of Fractal Aggregates: A Review. *Aerosol Sci. Technol.* **2011**, *45*, 765−779.

(28) Meakin, P. Diffusion-Limited Aggregation in Three Dimensions: Results from a New Cluster-Cluster Aggregation Model. *J. Colloid Interface Sci.* **1984**, *102*, 491−504.

(29) Cai, J.; Lu, N.; Sorensen, C. M. Analysis of Fractal Cluster Morphology Parameters: Structural Coefficient and Density Autocorrelation Function Cutoff. *J. Colloid Interface Sci.* **1995**, *171*, 470−473.

(30) Sorensen, C. M.; Cai, J.; Lu, N. Light-Scattering Measurements of Monomer Size, Monomers per Aggregate, and Fractal Dimension for Soot Aggregates in Flames. *Appl. Opt.* **1992**, *31*, 6547−6557.

(31) Kilps, J. R.; Logan, B. E.; Alldredge, A. L. Fractal Dimensions of Marine Snow Determined from Image Analysis of In Situ Photographs. *Deep Sea Res., Part I* **1994**, *41*, 1159−1169.

(32) Jungblut, S.; Joswig, J.-O.; Eychmüller, A. Diffusion- and Reaction-Limited Cluster Aggregation Revisited. *Phys. Chem. Chem. Phys.* **2019**, *21*, 5723−5729.

(33) Kim, K. S.; Kim, C.; Karniadakis, G. E.; Lee, E. K.; Kozak, J. J. Density-Dependent Finite System-Size Effects in Equilibrium Molecular Dynamics Estimation of Shear Viscosity: Hydrodynamic and Configurational Study. *J. Chem. Phys.* **2019**, *151*, 104101.

(34) Lee, J. H.; Kim, C.; Colvin, M. E. Molecular Dynamics Studies of the Melting Kinetics of Superheated Crystals. *J. Phys. Chem. C* **2022**, *126*, 4199.
(35) Rotne, J.; Prager, S. Variational Treatment of Hydrodynamic Interaction in Polymers. *J. Chem. Phys.* **1969**, *50*, 4831−4837.
(36) Yamakawa, H. Transport Properties of Polymer Chains in Dilute Solution: Hydrodynamic Interaction. *J. Chem. Phys.* **1970**, *53*, 436−443.
(37) Lin, M. Y.; Lindsay, H. M.; Weitz, D. A.; Ball, R. C.; Klein, R.; Meakin, P. Universal Reaction-Limited Colloid Aggregation. *Phys. Rev. A: At., Mol., Opt. Phys.* **1990**, *41*, 2005−2020.
(38) Derjaguin, B.; Landau, L. Theory of the Stability of Strongly Charged Lyophobic Sols and of the Adhesion of Strongly Charged Particles in Solutions of Electrolytes. *Acta Physicochim. URSS* **1941**, *43*, 30−59.
(39) Liang, Z.; Gimbutas, Z.; Greengard, L.; Huang, J.; Jiang, J. A fast multipole method for the Rotne−Prager−Yamakawa tensor and its applications. *J. Comput. Phys.* **2013**, *234*, 133−139.
(40) Carrasco, B.; García de la Torre, J. Improved hydrodynamic interaction in macromolecular bead models. *J. Chem. Phys.* **1999**, *111*, 4817−4826.
(41) Schmidt, R. R.; Cifre, J. G.; de la Torre, J. Comparison of Brownian dynamics algorithms with hydrodynamic interaction. *J. Chem. Phys.* **2011**, *135*, 084116.
(42) Ziervogel, K.; Forster, S. Aggregation and Sinking Behaviour of Resuspended Fluffy Layer Material. *Cont. Shelf Res.* **2005**, *25*, 1853−1863.
(43) Jackson, G. A.; Burd, A. B. Aggregation in the Marine Environment. *Environ. Sci. Technol.* **1998**, *32*, 2805−2814.
(44) Alldredge, A. L.; Cowles, T. J.; MacIntyre, S.; Rines, J. E. B.; Donaghay, P. L.; Greenlaw, C. F.; Holliday, D. V.; Dekshenieks, M. M.; Sullivan, J. M.; Zaneveld, J. R. V. Occurrence and Mechanisms of Formation of a Dramatic Thin Layer of Marine Snow in a Shallow Pacific Fjord. *Mar. Ecol.: Prog. Ser.* **2002**, *233*, 1−12.

https://doi.org/10.1021/acsomega.2c03547
ACS Omega 2022, 7, 40826−40835